Pharm Res (2013) 30:2891–2901
DOI 10.1007/s11095-013-1120-6

RESEARCH PAPER

Aerosol Delivery of Nanoparticles in Uniform Mannitol Carriers Formulated by Ultrasonic Spray Freeze Drying

Suzanne M. D'Addio • John Gar Yan Chan • Philip Chi Lip Kwok • Bryan R. Benson • Robert K. Prud'homme • Hak-Kim Chan

Received: 8 March 2013 / Accepted: 11 June 2013 / Published online: 27 July 2013

ABSTRACT

Purpose While most examples of nanoparticle therapeutics have involved parenteral or IV administration, pulmonary delivery is an attractive alternative, especially to target and treat local infections and diseases of the lungs. We describe a successful dry powder formulation which is capable of delivering nanoparticles to the lungs with good aerosolization properties, high loadings of nanoparticles, and limited irreversible aggregation.

Methods Aerosolizable mannitol carrier particles that encapsulate nanoparticles with dense PEG coatings were prepared by a combination of ultrasonic atomization and spray freeze drying. This process was contrasted to particle formation by conventional spray drying.

Results Spray freeze drying a solution of nanoparticles and mannitol (2 wt% solids) resulted in particles with an average diameter of $2 1 \pm 1.7\,\mu$m, regardless of the fraction of nanoparticles loaded (0–50% of total solids). Spray freeze dried (SFD) powders with a 50% nanoparticle loading had a fine particle fraction (FPF) of 60%. After formulation in a mannitol matrix, nanoparticles redispersed in water to $< 1\,\mu$m with hand agitation and to < 250 nm with the aid of sonication. Powder production by spray drying was less successful, with low powder yields and extensive, irreversible aggregation of nanoparticles evident upon rehydration.

Conclusions This study reveals the unique advantages of processing by ultrasonic spray freeze drying to produce aerosol dry powders with controlled properties for the delivery of therapeutic nanoparticles to the lungs.

KEY WORDS drug delivery · nanoparticle aerosol carriers · NPAC · spray drying · spray freeze drying

ABBREVIATIONS

d_a	Aerodynamic diameter
DPI	Dry powder inhaler
EtTP-5	2,2,10,10-tetraethyl-6,14-bis (triisopropylsilylethynyl)- 1,3,9,11-tetraoxadicyclopenta [b,m] pentacene fluorescent dye
FPF	Fine particle fraction
LN2	Liquid nitrogen
NGI	Next generation impactor
NP	Nanoparticle
NPAC	NP aerosol carriers
$PLA_{3.8k}$-*b*-PEG_{5k}-OCH_3	Polylactide-*b*-poly(ethylene glycol)
PSD	Particle size distribution
PVA	Polyvinyl alcohol
SD	Spray dry
SFD	Spray freeze dry
THF	Tetrahydrofuran

Electronic supplementary material The online version of this article (doi:10.1007/s11095-013-1120-6) contains supplementary material, which is available to authorized users.

S. M. D'Addio • J. G. Y. Chan • P. C. L. Kwok • H.-K. Chan (✉)
Advanced Drug Delivery Group, Faculty of Pharmacy
The University of Sydney, Pharmacy Building A15,
Camperdown, New South Wales 2006, Australia
e-mail: kim.chan@sydney.edu.au

S. M. D'Addio • B. R. Benson • R. K. Prud'homme (✉)
Chemical and Biological Engineering
Princeton University, Princeton, New Jersey 08854, USA
e-mail: prudhomm@princeton.edu

Present Address:
P. C. L. Kwok
Department of Pharmacology and Pharmacy, LKS Faculty
of Medicine The University of Hong Kong, Hong Kong, SAR

INTRODUCTION

Delivery of therapeutics by aerosol inhalation is an attractive strategy to address diseases of the lungs like COPD, lung cancer, and infections (1) and has the potential to maximize drug concentrations at the disease site and minimize off-target exposure of healthy tissue. There is interest in specifically incorporating drug nanoparticles into aerosol drug delivery formulations to treat local diseases in the lungs because they are of an appropriate size to escape nonspecific clearance and enable sustained release. Oberdorster has shown that insoluble nanoparticles in the size range of 100–200 nm are retained in the lungs for extended times relative to micron-sized particles, which are more rapidly cleared by either mucoscilliary or macrophage action (2, 3). However, objects smaller than ~30 nm are rapidly cleared by transport through the endothelial lining into the circulatory system, as has been demonstrated by insulin delivery by aerosol inhalation (4). A successful strategy for delivering NPs would have applicability to the many poorly water soluble drug compounds being discovered by high throughput methods.

Nanoparticles can be delivered by aerosolization as a liquid suspension or a dry powder, though both approaches have associated challenges. Nanoparticle suspensions prepared in aqueous media to be administered in nebulized droplets require long-term stability. While in dry form nanoparticle size can be retained, in aqueous media the high surface energy and interfacial area of nanoparticles presents major challenges in preventing particle size changes by Ostwald ripening or secondary crystallization. A dry powder formulation stabilizes the nanoparticles, but nanoparticle dry powders are poorly dispersed by dry powder inhalers (DPIs) and metered dose inhalers (MDIs) due to the strong cohesive forces between nanometer-sized particles; therefore, strategies to incorporate nanoparticles into larger carrier particles are of interest.

Successful NP delivery *via* dry powder aerosol administration presents several challenges. First, the NPs must be formulated into a larger particle form to avoid cohesive aggregation. Second, the powders must have sizes that promote delivery to the deep lung while also containing high loadings of NPs. The efficiency of powder delivery to the lungs by inhalation of dry powders is based on particle aerodynamic properties. For spherical particles, the aerodynamic diameter, d_a, is a function of the geometric size and the average density of the particle (5). Particles with $d_a \leq 5$ μm are considered to be suitable for deposition in the lungs. Solid particles in this size range are often still too cohesive to be directly aerosolized (6). Edwards *et al.* found that large, porous particles have better aerosolization properties than small, dense particles with equivalent d_a (7), which is due to the reduced adhesive contacts between more corrugated particles (8, 9). An additional consideration for aerosol carriers is that the NPs must be redispersed back to NP size once deposited in the lungs. Aggregation of NPs during spray drying has been observed, where the resulting powder could be aerosolized but the NPs could not be redispersed back to nanometer sizes (10). Protection from aggregation is a function both of the intrinsic stabilizing surface coating on the NP and of a matrix phase that minimizes direct particle contact during drying. While NP contacts can be minimized by dilution with the matrix material, this dilution compromises drug loading.

In this work, we capitalize on the different mechanisms of particle formation in spray freeze drying and spray drying to form aerosolizable particles with high loadings of NPs with limited aggregation. We refer to these composite particles as NP aerosol carriers (NPACs). In spray drying (11), the powder size and morphology depend on the relative rate of evaporation, κ, and solute diffusion, D_i. Solid, spherical particles are produced when diffusion is dominant, but when evaporation is fast, there is solute or NP enrichment at the droplet surface and buckling or crumpling of the particle is observed upon drying (10, 12). The large disparity in diffusion coefficients for the molecularly dissolved matrix materials and the dispersed NPs causes segregation of components in the final dried particle (10) which can contribute to irreversible aggregation of NPs (13). In contrast, spray freeze drying (14) is based on rapidly trapping the solute in a frozen droplet prior to lyophilization. The rapid freezing step limits the amount of solute diffusion that can occur, which can decrease the potential for NPs to aggregate.

Recent work by the Hadinoto group has evaluated the production of NPACs by spray freeze drying using a two fluid nozzle for atomization, where the loading of lipid-polymer hybrid NPs into mannose, mannose/leucine, PVA, and PVA/leucine particles was investigated with a focus on NP loading, redispersion, and aerosolization efficiency (15–17). Droplet formation with the two fluid nozzle is not uniform and leads to a relatively broad dry particle size; the best FPF achieved was 32% by this method (17). Ultrasonic atomization, in which the drop breakup is driven by the ultrasonic pressure wave, generates much more uniform drop sizes and final particle sizes. We have obtained FPFs as high as 60% for mannitol and lysozyme solutions, and the aqueous solution composition had a minimal effect on atomization (18).

The objective of this work is to compare the properties of NP-containing powders prepared by conventional spray drying *versus* spray freeze drying with ultrasonic atomization. Of particular importance is the characterization of NP redispersibility and whether redispersibility varies with NP loading. To form NPs, we use the Flash NanoPrecipitation process, which is suited to the formation of NPs with high

payloads of a variety of therapeutic and imaging agents *via* supersaturation and directed assembly (19–29). We have used generic protocols based on prior characterization of spray freeze dried powders prepared by ultrasonic atomization and not optimized the device or dosing level, which should be tailored to the specific demands of the therapy.

MATERIALS AND METHODS

Flash NanoPrecipitation (FNP)

For this study, model nanoparticles (NP) with a cholesterol core (Sigma Aldrich. St. Louis, MO, USA) stabilized by polylactide-*b*-poly(ethylene glycol) ($PLA_{3.8k}$-*b*-PEG_{5k}-OCH_3. Evonik. Birmingham, AL, USA) were prepared with a confined impinging jets mixer in which 1 or 5 ml of a solution of cholesterol (100 mg ml^{-1}) and PEG_{5k}-*b*-$PLA_{3.8k}$-OCH_3 (100- mg ml^{-1}) in THF was mixed against 1 or 5 ml of water and collected in 18 or 90 ml of stirred water (30). The final suspension was 5% THF, which was removed by dialysis in 3.5 kDa MWCO-dialysis tubing (Spectra/Por Regenerated Cellulose Dialysis Tubing. Cole Parmer, Chatswood, NSW, Australia) against 1 l of continuously stirred water, which was refreshed 3 times over 6 h.

Surfactant-free poly methyl methacrylate NPs (280 nm, 50 wt%. Arkema Inc. King of Prussia, PA, USA) were diluted in water to 3 wt% and imbibed with the fluorescent dye, 2,2,10,10-tetraethyl-6,14-bis(triisopropylsilylethynyl)-1,3,9,11-tetraoxadicyclopenta[b,m]pentacene (EtTP-5) (31). The latex particles were mixed with an equal volume of EtTP-5 in THF (1 mg ml^{-1}) to obtain a 50 vol% THF aqueous solution. After 10 min, THF was removed by rotary evaporation at 30°C and 100 Torr. Crystalline EtTP-5 precipitates were removed by filtration with a 2.7 μm cellulose filter. The final concentration of latex spheres in the solution was determined using thermogravimetric analysis (Perkin Elmer TGA 7. Waltham, MA, USA).

Both cholesterol and latex suspensions were characterized by dynamic light scattering (ZetaSizer Nano ZS, Malvern Instruments. Worcestershire, UK) using the normal analysis mode in the data analysis software. Sizes are reported using intensity-weighted averages. A sample was diluted in DI water until transparent, and each dilution was measured 2–3 times, where the measurement consisted of at least 10 cycles of data collection for 10s.

Spray Freeze Drying

Spray freeze dried (SFD) mannitol particles, cholesterol NP/mannitol particles, PEG_{4k}/mannitol particles, and fluorescent NP/mannitol particles were prepared by spray freeze drying the aqueous solutions in Table I. The solutions were fed *via* a digitally controlled syringe pump at 0.5 ml min^{-1} into a CV-24 ultrasonic nozzle powered by a Vibra Cell 40 kHz ultrasonic generator (Sono-Tek Corp., Milton, NY). The atomized droplets fell ~10 cm into the liquid nitrogen (LN_2) collection vessel. After spraying of the solution was complete, the excess LN_2 was allowed to boil off and the frozen droplets were lyophilized for 18 h on a shelf at 25°C (Christ Alpha 1–4 LOC-1 M, Martin Christ. Osterode am Harz, Germany).

Spray Drying

Spray Dried (SD) mannitol particles, cholesterol NP/mannitol particles, and fluorescent NP/mannitol were prepared with a Buchi 191 Mini Spray Dryer (Flawil, Switzerland). A two fluid nozzle was used to atomize the aqueous solutions in Table II. The mannitol solutions (SD03–SD07) were fed at a rate of 1.4 ml min^{-1} and were atomized with compressed air at 750–800 l hr^{-1} and an aspiration rate of 38 m^3 hr^{-1} (32). The inlet and outlet temperatures of the spray dryer were 110°C and 75°C, respectively. Mixtures of mannitol and NPs in deionized water (SD01–SD02) were spray dried with a solution feed rate of 1.4 ml min^{-1} and with compressed air at 400 l hr^{-1} and an aspiration rate of 38 m^3 hr^{-1}. The reduced air pressure was required to improve upon the poor yield of powder collected by the cyclone with the air flow of 750–800 l hr^{-1}. Sufficient yields of spray dried particles could not be recovered for Formulation SD01 (10 mg ml^{-1} NPs + 10 mg ml^{-1} mannitol) even under this reduce air flow rate. The concentration of mannitol was increased, as in formulation SD09, to improve yield.

Particle Sizing by Laser Diffraction

Volume-weighted particle size distributions of the dried powders were measured by dispersion in a 1 bar air stream of a Scirocco 2000 dry powder feeder (Malvern. Worcestershire, UK) and then sized by a Mastersizer 2000 (Malvern. Worcestershire, UK) using an obscuration between 0.3% and 10%. For the analysis, the optical properties of mannitol were set to be 1.433 and 0.1 for the real and imaginary refractive indices, respectively. The dispersant (air) refractive index was set to 1.000.

Particle Imaging

Images of dried powders were obtained using a field emission scanning electron microscope (SEM) (Zeiss Ultra Plus, Carl Zeiss NTS GmbH. Oberkochen, Germany) at 2 kV. The samples were prepared on carbon tape and sputter coated with approximately 11.3 nm palladium/gold using a K550X sputter coater (Quorum Emitech. Kent, UK) before imaging.

Table I Aqueous Solutions/Suspensions Used to Prepare Particles by Spray Freeze Drying with Ultrasonic Atomization

Formulation	Aqueous composition		
	Mannitol (mg ml^{-1})	Second component	Second component concentration (mg ml^{-1})
SFD01	10	cholesterol NPs	10
SFD02	19.4	cholesterol NPs	0.6
SFD03	20	–	–
SFD04	10	–	–
SFD05	40	–	–
SFD06	50	–	–
SFD07	10	fluorescent PS NPs	1×10^{-2}
SFD09	10	PEG_{4k}	0.5
SFD10	10	PEG_{4k}	3
SFD11	10	PEG_{4k}	18

Particle Dispersion

The fine particle fraction (FPF) of the 1:1 mannitol/NP powder was measured using a Next Generation Impactor (NGI) (Copley Scientific. Nottingham, UK). Particles dispersed in an air stream are conveyed through the instrument and impact on the eight consecutive stages based on the well-characterized aerodynamic size cutoffs. Before each run, all stages were coated with silicone spray (Slipicone, DC Products. Waverly, VIC, Australia) to minimize bouncing. The flow rate through the NGI was set to 100 l min^{-1} using a rotary vane vacuum pump (Model RA 0025 F 505, Busch. Maulburg, Germany) and calibrated flow meter (TSI 3063, TSI Instruments Ltd. Buckinghamshire, UK). At this condition, the aerodynamic diameter cut-off for particles captured on stages S1, S2, S3, S4, S5, S6 and S7 are 6.1, 3.4, 2.2, 1.3, 0.7, 0.4 and 0.2 μm, respectively. A filled capsule, containing 2.5–5 mg of powder, was placed into the sample compartment of an Aerolizer® DPI (Plastiape S.p.A, Osnago, Italy), the inhaler was activated, inserted into a United States Pharmacopoeia (USP) throat (33), and tested for 2.5 s at 100 l min^{-1}(34). After the run, the inhaler, capsule, throat, and all sample stages were washed with 4 ml of water. The solution was filtered with a 0.01 μm syringe tip filter and the filtrate was assayed for mannitol concentration by HPLC as described below. Tests of deposition were done in triplicate.

Table II Aqueous Solutions/Suspensions Used to Prepare Particles by Spray Drying with a Two Fluid Nozzle

Formulation	Aqueous composition		
	Mannitol (mg ml^{-1})	Second component	Second component concentration (mg ml^{-1})
SD01	10	cholesterol NPs	10
SD02	19.4	cholesterol NPs	0.6
SD03	20	–	–
SD04	10	–	–
SD05	40	–	–
SD06	50	–	–
SD07	150	–	–
SD08	10	fluorescent PMMA NPs	1×10^{-2}
SD09	90	cholesterol NPs	10

High Performance Liquid Chromatography

Quantification of mannitol deposition on each stage in the NGI was performed using high performance liquid chromatography (HPLC) (Model LC-20, Shimadzu. Kyoto, Japan). For the assay, a refractive index detector (Model RID-10A, Shimadzu. Kyoto, Japan) was used. Samples were filtered through a 0.01 μm filter and injected (100 μl) into a Resolve C-18 column, 5 μm, 150 mm × 3.9 mm (Waters. Milford, MA), with de-ionized, filtered water as mobile phase, at a flow rate of 1 ml min^{-1}. A calibration curve was constructed using standard solutions from 1 μg ml^{-1} to 1,000 μg ml^{-1}.

Differential Scanning Calorimetry (DSC)

The thermal properties the spray freeze dried powders were analyzed using a differential scanning calorimeter (DSC, Model 821e, Mettler Toledo. Greifensee, Switzerland). Samples (3–5 mg) were crimp-sealed in 40 μl aluminum crucibles, with a vent hole in the lid, and heated from 30°C to 180°C at a heating rate of 10°C min^{-1} under 250 cm^3-min^{-1} nitrogen purge.

X-Ray Diffraction (XRD)

Diffraction patterns for spray freeze dried powders were characterized using X-ray powder diffraction (D5000, Siemans. Munich, Germany). Samples for XRD were spread on glass slides and subjected to Cu Kα radiation at 30 mA and 40 kV. The scattered intensity was collected by a detector at 5–40° 2θ, at a step rate of 0.04° 2θ s^{-1}.

NP Redispersion

Cholesterol NPs, dried in a mannitol matrix by spray freeze drying or spray drying, were rehydrated by adding 5 ml of water to 50 mg of dried powder. The powder was shaken manually for 30 s and a size measurement was made by dynamic light scattering. The sample was then subjected to 1 min of sonication in a bath sonicator at room temperature and a second size measurement was made.

Confocal Laser Scanning Imaging

Dried powders were dispersed in 10 cSt silicone oil (Dow Corning 200® Fluid. Aldrich, St. Louis, MO, USA.) by hand agitation immediately before imaging. Confocal microscope images were obtained using a Leica TCS SP5 with a HCX PL APO 63.0x1.30 glycerine objective lens at 60X magnification. The EtTP-5 fluorescent dye in the NPs was excited with an argon lamp and the emission in the band 600–725 nm was collected.

RESULTS

NPAC Formation by Ultrasonic Spray Freeze Drying

An aqueous suspension of cholesterol NPs stabilized by $PLA_{3.8}$-*b*-PEG_{5k}-OCH_3 at 1 wt% total solids was prepared by Flash NanoPrecipitation (FNP). The cholesterol NPs had an average diameter of 80 nm and were narrowly distributed (Fig. 1 inset). The aqueous NP suspensions with dissolved mannitol (2 wt% solids) were spray freeze dried to obtain NPACs loaded with 50 wt% (SFD01) 3 wt% (SFD02), 0 wt% (SFD03) cholesterol NPs. The particle size distributions of the spray freeze dried powders for these three formulations were nearly identical, despite the different loadings of NPs (Fig. 1). This is an attribute of the spray freezing process where the final particle size reflects the sizes of the original liquid drops. Each of the distributions had a shoulder off the main peak, corresponding to small fragments of mannitol. Since fragments skew the volume weighted particle size distribution, we report the mode of the distribution (d_{mode}). The average d_{mode} for formulations SFD01, SFD02, and SFD03 shown in Fig. 1a was 21 ± 1.7 μm.

SEM Imaging

A representative electron micrograph of formulation SFD01 in Fig. 2a shows the spherical and highly porous nature of the NPACs. Under high magnification, the particle has submicron pores (Fig. 2b). Aggregates of the typical nanorod crystals of mannitol (32) can be seen in spray particles of SFD mannitol under high magnification (18), but this feature is lacking in the NP-loaded formulation.

Powder Dispersion

After powder deposition in the NGI, recovery by dissolution, filtration, and quantification of powder deposition on each stage using HPLC, the mass recovery of mannitol (sample SFD01) was 60%. The distribution of mannitol mass on the stages of the NGI is graphed in Fig. 1b. The cumulative fraction of particles with $d_a \leq 5$ μm, corresponding to the Fine Particle Fraction (FPF), was determined by interpolation. The FPF of the recovered dose was 60 ± 13%, which is in the range previously obtained for pure mannitol particles produced from a 1–2 wt% solution by ultrasonic atomization and spray freeze drying (18).

XRD

Powder XRD patterns for raw mannitol, cholesterol, and $PLA_{3.8}$-*b*-PEG_{5k}-OCH_3 were obtained for comparison to the pattern for the spray freeze dried powders (Fig. 1c). In the NPAC (SFD01), the crystal peaks of cholesterol were not observed, but two broad peaks from $PLA_{3.8}$-*b*-PEG_{5k}-OCH_3 were present at 19.2° 2θ and 23.5° 2θ. Many of the major peaks corresponding to the mannitol crystals were absent and a strong peak appears at 9.75° 2θ, which was not observed in the raw mannitol sample. A 3:1 mannitol/PEG_{4k} formulation (SFD10) was spray freeze dried, which replicated the relative ratios of these components in SFD01. The powder diffraction pattern had two broad peaks at 19° 2θ and 23° 2θ corresponding to PEG, which was also seen in the diffraction pattern for SFD01. The peak at 9.75° 2θ was also present. This pattern is observed for other ratios of spray freeze dried PEG_{4k} and mannitol (SFD09 and SFD11, Supplementary Material).

DSC

NPACs were characterized by DSC (Fig. 1d). Mannitol displayed one endothermic event, corresponding to the crystal melting from 160°C to 175°C. In the DSC heating trace for SFD01 (1:1 mannitol/NP) an endotherm from 50°C to 60°C corresponded to PEG melting and another endotherm from 138°C to 150°C corresponded to the melting of crystalline cholesterol. Prior to the mannitol melting peak, there was an additional endothermic and exothermic event from 145°C to 160°C. After allowing the sample to cool to room temperature, the same sample was subjected to the same temperature ramp, denoted as Scan 2. The melting peaks for PEG, cholesterol, and mannitol were observed, but the event from 145°C to 160°C was not. For SFD10, PEG melting from 50°C to 60°C, mannitol melting from 160°C to 175°C and the endothermic and exothermic transition at 145–160°C were observed, without being obscured by the melting of cholesterol, which was not present in this preparation. As with the NPACs, this transition was irreversible and only observed on Scan 1. The additional PEG_{4k}/mannitol samples with different relative weight ratios (SFD09 and SFD11) were also characterized by DSC (Supplementary Material) and similar features were observed in the DSC trace for Scan 1 and Scan 2.

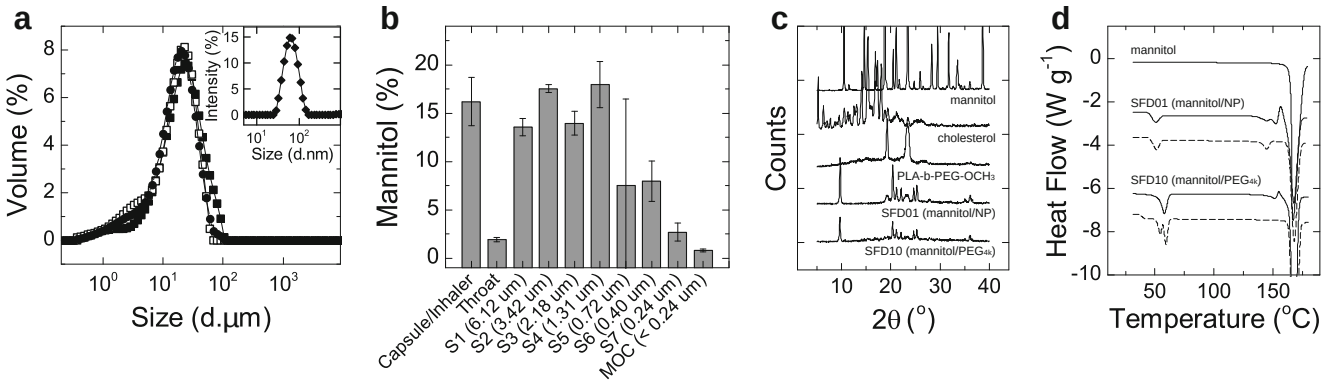

Fig. 1 Characterization of PNACs formed by SFD. (**a**) Volume weighted particle size distributions for mannitol NPAC particles prepared by SFD with ultrasonic atomization for formulations (■) SFD01 (50 wt% cholesterol NPs), (□) SFD02 (3 wt% cholesterol NPs), and (●) SFD03 (0% cholesterol NPs). Inset: Intensity weighted particle size distribution for (♦) cholesterol NPs. (**b**) Impaction data for SFD01 dispersed at 100 l min^{-1} in the Aerolizer®, where the fraction of the recovered mannitol dose administered is plotted for each stage in the NGI. S1 to S7 denote impactor stages 1 to 7, followed by the aerodynamic cutoff diameter. MOC is the micro-orifice collector. Error bars are the standard deviation for $n = 2$ replicates. (**c**) From top to bottom, powder XRD patterns for the mannitol, cholesterol, $PLA_{3.8k}$-*b*-PEG_{5k}-OCH_3, SFD01, and SFD10 (mannitol/PEG_{4k}). (**d**) DSC traces, obtained by heating samples at 10°C min^{-1}, where the solid line is the first heating trace and the dashed line is a second heating trace carried out on the same sample after allowing it to cool to room temperature.

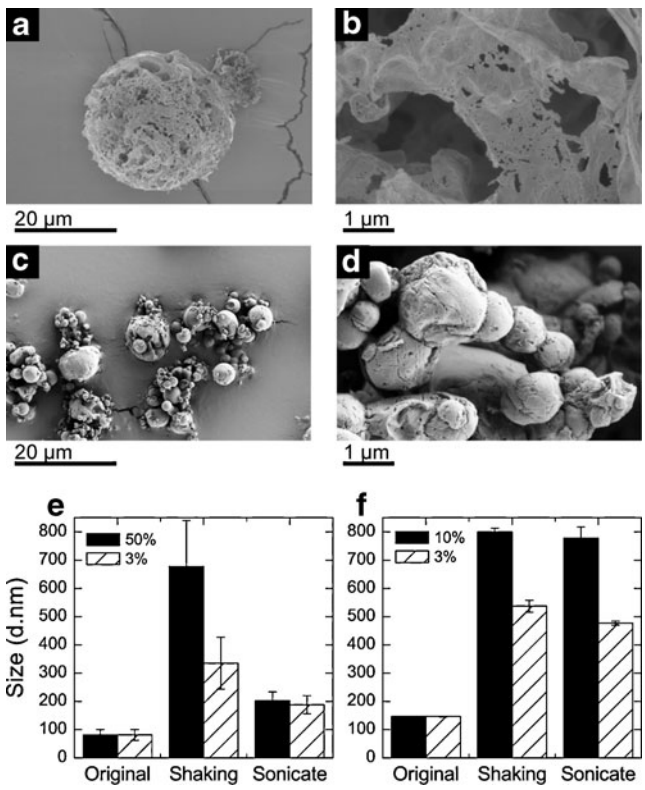

Fig. 2 NPACs formed by SFD and SD. (**a**) SEM micrograph of a typical particle in formulation SFD01, loaded with 50% cholesterol NPs by mass. (**b**) High magnification of SFD01. (**c**) SEM micrographs of SD01, prepared with 1:1 NP/mannitol (**d**) High magnification of SD01 (**e**) Z-average particle sizes of the resuspended NPs, dried by spray freeze drying with loading of 50% NPs by mass (*black bars*) or 3% NPs by mass (*hashed bars*). (**f**) Z-average particle sizes of the resuspended NPs, dried by spray drying with loading of 10% NPs by mass (*black bars*) or 3% NPs by mass (*hashed bars*).

NPAC Formation by Spray Drying

Spray dried NPACs of cholesterol NPs (180 nm) with mannitol as a carrier matrix were prepared in Formulations SD01 and SD02 (Table II), using the same aqueous solution compositions that were used in spray freeze drying formulations SFD01 and SFD02. For feed solution of 2 wt% solids, small particle size and dilute concentration resulted in poor recovery of the dried powders. Enough of SD02 was collected for characterization and dissolution experiments. The recovery of SD01 (1:1 NP/mannitol) was extremely poor (<10 mg, *i.e.* less than 2%) and only enough sample for electron microscopy was obtained. The electron micrographs for these two samples are presented in Fig. 2c–d. At low magnification, a few particles with sizes of 5–10 μm can be observed; however, smaller 1 μm particles predominate. At 50 K times magnification these small particles appear to be dense, and without nanoscale features of mannitol crystals observed in the pure mannitol spray dried particles (Fig. 2d).

Redispersion of NPs from NPACs

To demonstrate the release of NPs upon dissolution of the mannitol matrix, a sample of each powder was rehydrated at a concentration of 10 mg ml^{-1}, and shaken for 30 s. A drop of the suspension was diluted in water, and a size measurement was taken. The suspension was then sonicated in a bath sonicator for 1 min, diluted, and another size measurement was taken. DLS size measurements were repeated at least three times. The average size after dissolution was compared to the original NP size prior to SFD or SD (Fig. 2e–f). At 50% loading, redispersion by hand agitation of the particles formed by SFD (Fig. 2e) demonstrated some aggregation;

the average size was 680 nm. At 3% NP loading, the NPs redispersed to below 400 nm with simple shaking. With additional energy input by sonication, the particles in both formulations redispersed to below 200 nm. Since the recovery of formulation SD01 (Table II) was insufficient for dissolution testing, 10% loaded NP/mannitol particles were prepared by spray drying a suspension of 10 mg ml^{-1} NPs with 90 mg ml^{-1} mannitol (SD10, Table II). The recovery was improved significantly by increasing the concentration of mannitol (>400 mg). Upon dissolution with hand agitation, 10% and 3% spray dried NP/mannitol formulations yielded NP aggregates, with sizes of 800 nm and 540 nm, respectively. In contrast to the SFD particles, bath sonication had no effect on the redispersion of NPs from SD particles.

Mannitol Powder Preparation by SFD and SD

Mannitol powders without NPs were prepared by both SFD (SFD03-SFD06, Table I) and SD (SD03-SD07, Table II) for comparison. The average diameter for the particle size distribution, D_{50}, for each formulation is plotted in Fig. 3a–b as a function of the aqueous solution concentration of mannitol used to prepare the particles. The diameter of particles prepared by SD is linearly dependent on the feed solution concentration, c_s, (Fig. 3a, $p=0.006$) and varies between 1 μm and 4 μm. This is in contrast to the average size of particles produced by ultrasonic atomization and SFD, where there is essentially no dependence of the D_{50} on the feed solution concentration ($p=0.4$). The sizes are ~21 μm. The standard error of the sizes measured for the SFD particles is due to variability in multiple measurements due to the fragmentation of the particles (18). Micrographs of the mannitol powders prepared by SFD and SD are presented in Fig. 3c–d. For particles formulated at the same concentration in both processes, a five to ten-fold decreased particle size is obtained by SD relative to SFD. There are also a large number of smaller particles observed in micrographs of the SD samples. The SFD particles are more porous and corrugated than the SD particles, which have smooth, continuous surfaces.

NP Distribution in Mannitol Powders

Formulations SFD07 and SD08 were prepared with dilute concentrations of fluorescent latex spheres in order to visualize the distribution of NPs in the powders formed by SFD or SD. The distribution of the fluorescent NPs in powders were characterized by confocal scanning microscopy and bright field microscopy. The bright field images of the spray dried mannitol powders (Fig. 4a) correspond well with the SEM images of SD mannitol in Figs. 2c and 3d; the primary particles are 1–2 μm spherical, smooth, and form larger aggregates. The fluorescence from the NPs emanates mostly from large clusters with sizes > ~500 nm (Fig. 4c). The bright field images of SFD formulation (Fig. 4b) are poorly resolved since the particle dimensions are much larger than the focal plane of the image. The fluorescence obtained for SFD08, the SFD formulation, shows fluorescence distributed essentially uniformly throughout the particle structure (Fig. 4d).

DISCUSSION

We have investigated the formation of NP-loaded aerosol carriers (NPACs) by spray freeze drying (SFD) with ultrasonic atomization *versus* conventional spray drying (SD). These carriers are intended for use as aerosolizable delivery vehicles to deposit NPs in the lungs for therapy. Deposition of NPACs in the lungs and therapeutic delivery of the NPs requires control of the aerodynamic FPF and then release of the encapsulated NPs from the soluble matrix deposited in the lungs. Oberdorster has shown that insoluble ultrafine particles are most slowly cleared from the lungs relative to larger particles and aggregates (2). If the goal is extended release in the lungs, then retention of NP size is important. Our results show the issues involved in the optimization of NPAC size and NP aggregation between the two spraying techniques. The key issues are: (1) processing and powder recovery, (2) aerosolization of the NPAC, (3) release of submicron NPs in the lungs, and (4) the crystal form of mannitol produced by each process.

Processing and powder recovery

The inevitable size distribution for particles produced by conventional two-fluid atomizers and conventional SD means that the sub-5 μm size required to maximize FPF compromises the recovery efficiency in the production process. We obtained poorer solids recovery with conventional SD than with the SFD process, even though the SFD particles also had aerodynamic diameters of 5 μm. The high loading of NPs did not significantly affect particle size (21 μm), porosity (Fig. 2a), or aerosolization (Fig. 1b), compared to the formulation with pure mannitol which was previously studied (18).

Aerosolization of the NPAC

The NPAC architecture is attractive for NP delivery since aerosolization can be controlled by engineering the NPs into larger structures (>1,000 nm) with properties conducive to good aerosolization and delivery to the deep lung (10). While it has been demonstrated that low density, crenellated powders can be produced by conventional SD (7), the relative rates of solvent evaporation, to solute diffusion, and solute concentration influences the final particle size, density, and morphology in a complex way (12). Fast drying is desired to obtain large porous particle morphologies, but the work of

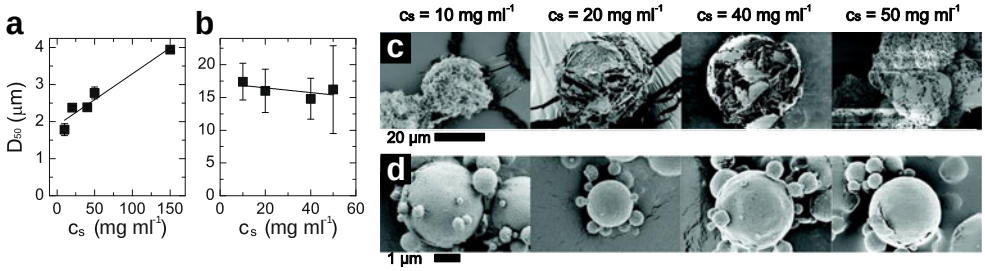

Fig. 3 Spray drying *vs.* spray freeze drying mannitol. Effect of varying solute concentration, c_s, on the median particle size, d_{50}, measured by laser light scattering in both (**a**) spray drying and (**b**) spray freeze drying processes. Each point is the average of three measurements, and the error bars correspond to the standard deviation of the mean. SEM images of mannitol particles produced by (**c**) spray freeze drying and (**d**) spray drying.

Sung *et al.* revealed that the slower diffusion of the NPs relative to that of solute molecules (*i.e.* L-leucine) resulted in powders enriched with NPs at the receding droplet surface during drying, which caused particle fracture and deformation (35).

SFD is advantageous over SD to form NPACs because control over particle size and porosity is decoupled. Freezing occurs faster than diffusion of solutes in the droplets, effectively trapping solids in a porous, homogenous structure (Fig. 4f). The frozen droplet occupies a volume similar to the original aqueous droplet, allowing the final particle size to be controlled through the size of the aqueous droplet. Specifically using ultrasonic atomization produces droplets of constant size, where the size of the droplets produced is dominated by the frequency of the nozzle and is only weakly affected by the properties of the liquid (Fig. 3b) (36). In this

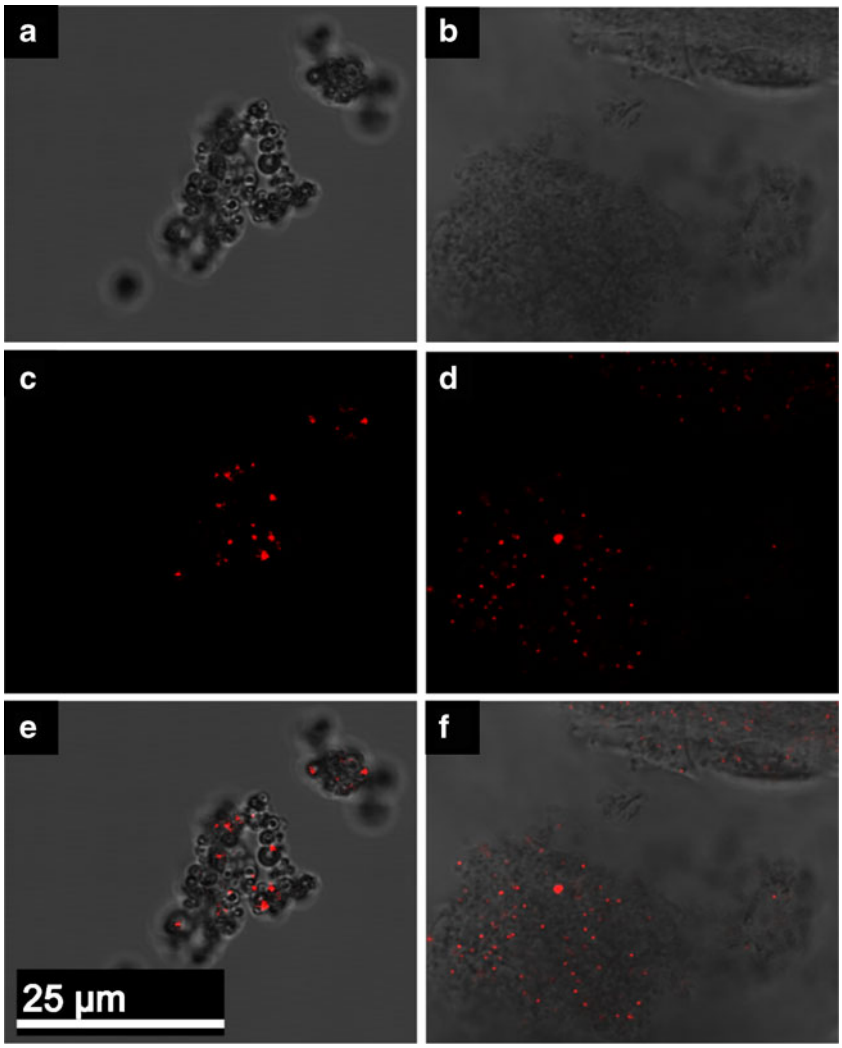

Fig. 4 Phase contrast (**a**, **b**), confocal fluorescence (**c**, **d**), and overlaid images (**e**, **f**) for mannitol particles spray dried (*left column*) and spray freeze dried (*right column*) with fluorescent latex NPs.

paper, aqueous solutions of mannitol and NPs with a total concentration of 2 wt% solids were SFD, and the relative ratios of NPs to mannitol were varied. When the cholesterol NPs were incorporated into carriers to form NPACs, the size of SFD particles did not change appreciably, even for loadings of NPs as high as 50% (Fig. 1a). After lyophilization, the resulting large particle had a porous structure (Fig. 2a–b), good aerosol properties (Fig. 1b), with a quantified FPF of 60%.

Release of submicron NPs in the lungs

While we have not performed *in vivo* tests in this study, the combined interpretation of previous *in vivo* studies and the particle characterization performed on the NPAC allows reasonable conclusions to be drawn about NP delivery by particles produced by the two processes. Aggregation of NPs is undesirable because it can alter bioavailability and accelerate clearance (37). During conventional SD the slow diffusion of the NPs causes local concentration of NPs as seen in the fluorescence images in Fig. 4c. High NP concentrations favor aggregation, which was seen for both SD and SFD particles (Fig. 2e, f). However, the SD process is more susceptible to aggregation as indicated by the inability to redisperse SD particles produced at either 3 or 10% loadings, while powders with a 50% loading of NPs produced by SFD were broken up by mild sonication. The different responses to sonication between the SD and the SFD samples also point to the stronger aggregation that occurs during conventional drying. Whereas with the SFD samples the level of aggregation seen after hand agitation could be reduced, almost to the original NP size, by sonication, the SD NPs could not be redispersed even with sonication. This is not to indicate that sonication is a therapeutically relevant redispersion process, but it gives additional insight into the NP interactions that occur during drying. The NPs from the SFD process redispersed back to the nanoscale (~330 nm) in water with simple shaking at a 3% loading. This result showed quantitatively that solute diffusion results in clustering and irreversible aggregation of NPs during SD and that aggregation is minimized in SFD.

The crystal form of mannitol

The combination of mannitol and NPs into the dry powder formulation changed the mannitol polymorph. While spray freeze dried mannitol solutions yielded mannitol particles with the same β polymorph as the starting material (18), the strong peak at 9.75° 2θ in the NPAC powder diffraction pattern (Fig. 1c), and the irreversible recrystallization transition in the DCS trace (Fig. 1d) provides evidence of the formation of the δ polymorph of mannitol by SFD (38) which is thermodynamically unstable at ambient conditions. A similar diffraction pattern and irreversible thermal transition was observed for a SFD solution of 3:1 mannitol and PEG_{4k} (SFD10), which indicates the δ polymorph was obtained by rapidly precipitating mannitol by SFD in the presence of PEG. While the δ polymorph of mannitol has processing advantages for pharmaceutical formulation (38), polymorph uniformity and stability is critical in the regulatory approval process and the most thermodynamically stable polymorph is most often desirable. PEG was present in the NP formulation to impart long term colloidal stability in aqueous media and may not be required if the NPs are spray freeze dried within a few days of production and the formation of the δ mannitol polymorph can be avoided.

CONCLUSIONS

Spray freeze drying with ultrasonic atomization was compared to conventional spray drying for the formation of NP-loaded Aerosol Carriers (NPAC). The NPs used in this work were prepared by FNP, and were composed of a cholesterol core with a stabilizing $PLA_{3.8k}$-b-PEG_{5k}-OCH_3 layer, as a model for hydrophobic drug compounds which can be processed by FNP. NPs with a dense PEG corona (39) and a variety of hydrophobic payloads for imaging, therapy, and other uses have been produced by FNP (19–29). Since the stability is conferred by the PEG steric layer, it is anticipated that similar results by SD and SFD would be obtained with other API core materials. In this work, we have not optimized the device or dose to obtain the maximum FPF. These parameters would be tailored for a specific drug for a specific disease indication. When formulated into dried mannitol matrices by spray freeze drying (SFD), the NPs redispersed in water to a size < 200 nm with sonication, while processing by spray drying (SD) caused irreversible aggregation of the NPs. From the perspective of uniformity of NPAC particle size and the flexibility of controlling size and density, SFD has advantages over conventional SD. Also, SFD results in less NP aggregation which is significant for extended retention of NPs in the lungs. While extra cost or complexity of a sterile SFD process would have to be assessed based on the therapeutic advantages of the formulation, we note that Amgen has built and operated a pilot scale SFD plant which was designed for protein aerosol delivery (40). PEG caused the formation of an unstable mannitol crystal polymorph, and further investigation of excipient interactions during spray freeze drying should be performed. This work establishes that high loadings of NPs in a carrier matrix can be achieved by spray freeze drying with excellent aerosolization properties.

ACKNOWLEDGMENTS AND DISCLOSURES

This work made use of the Confocal & Electron Microscopy Core Facility at Princeton University and the authors

acknowledge Joe Goodhouse for expert help with confocal microscopy. This work was supported through National Science Foundation and the Australian Academy of Science as part of the East Asia and South Pacific Summer Institutes Fellowship (1015344) and through grants from the Australian Research Council (DP0985367 & 120102778).

REFERENCES

1. Weers JG, Bell J, Chan HK, Cipolla D, Dunbar C, Hickey AJ, et al. Pulmonary formulations: what remains to be done? J Aerosol Med Pulm Drug Deliv. 2010;23 Suppl 2:S5–23.
2. Oberdorster G, Sharp Z, Atudorei V, Elder A, Gelein R, Lunts A, et al. Extrapulmonary translocation of ultrafine carbon particles following whole-body inhalation exposure of rats. J Toxicol Env Heal A. 2002;65(20):1531–43.
3. Tabata Y, Ikada Y. Phagocytosis of polymer microspheres by macrophages. New Polymer Materials. Berlin: Springer; 1990. p. 107–41.
4. Wigley FW, Londono JH, Wood SH, Shipp JC, Waldman RH. Insulin across respiratory mucosae by aerosol delivery. Diabetes. 1971;20(8):552–6.
5. Hinds WC. Aerosol technology, properties, behaviors, and measurement of airborne particles. 2nd ed. New York: John Wiley & Sons, Inc; 1999.
6. Heyder J, Gebhart J, Rudolf G, Schiller CF, Stahlhofen W. Deposition of particles in the human respiratory-tract in the size range 0.005-15-Mu-M. J Aerosol Sci. 1986;17(5):811–25.
7. Edwards DA, Hanes J, Caponetti G, Hrkach J, BenJebria A, Eskew ML, et al. Large porous particles for pulmonary drug delivery. Science. 1997;276(5320):1868–71.
8. Chan HK, Chew NYK. Use of solid corrugated particles to enhance powder aerosol performance. Pharm Res. 2001;18(11):1570–7.
9. Kwok PC, Tunsirikongkon A, Glover W, Chan HK. Formation of protein nano-matrix particles with controlled surface architecture for respiratory drug delivery. Pharm Res. 2011;28(4):788–96. Epub 2010/12/08.
10. Tsapis N, Bennett D, Jackson B, Weitz DA, Edwards DA. Trojan particles: large porous carriers of nanoparticles for drug delivery. P Natl Acad Sci USA. 2002;99(19):12001–5.
11. Broadhead J, Rouan SKE, Rhodes CT. The spray drying of pharmaceuticals. Drug Dev Ind Pharm. 1992;18(11–12):1169–206.
12. Vehring R, Foss WR, Lechuga-Ballesteros D. Particle formation in spray drying. J Aerosol Sci. 2007;38(7):728–46.
13. Kho K, Cheow WS, Lie RH, Hadinoto K. Aqueous re-dispersibility of spray-dried antibiotic-loaded polycaprolactone nanoparticle aggregates for inhaled anti-biofilm therapy. Powder Technol. 2010;203(3):432–9.
14. Maa YF, Nguyen PA, Sweeney T, Shire SJ, Hsu CC. Protein inhalation powders: spray drying vs spray freeze drying. Pharm Res. 1999;16(2):249–54.
15. Cheow WS, Ng ML, Kho K, Hadinoto K. Spray-freeze-drying production of thermally sensitive polymeric nanoparticle aggregates for inhaled drug delivery: effect of freeze-drying adjuvants. Int J Pharm. 2011;404(1–2):289–300.
16. Wang Y, Kho K, Cheow WS, Hadinoto K. A comparison between spray drying and spray freeze drying for dry powder inhaler formulation of drug-loaded lipid-polymer hybrid nanoparticles. Int J Pharm. 2012;424(1–2):98–106.
17. Kho K, Hadinoto K. Optimizing aerosolization efficiency of dry-powder aggregates of thermally-sensitive polymeric nanoparticles produced by spray-freeze-drying. Powder Technol. 2011;214(1):169–76.
18. D'Addio SM, Chan JGY, Kwok PCL, Prud'homme RK, Chan HK. Constant size, variable density aerosol particles by ultrasonic spray freeze drying. Int J Pharm. 2012;427(2):185–91.
19. Akbulut M, Ginart P, Gindy ME, Theriault C, Chin KH, Soboyejo W, et al. Generic method of preparing multifunctional fluorescent nanoparticles using flash NanoPrecipitation. Adv Func Mater. 2009;19(5):718–25.
20. Ansell SM, Johnstone SA, Tardi PG, Lo L, Xie S, Shu Y, et al. Modulating the therapeutic activity of nanoparticle delivered paclitaxel by manipulating the hydrophobicity of prodrug conjugates. J Med Chem. 2008;51(11):3288–96.
21. Chen T, D'Addio SM, Kennedy MT, Swietlow A, Kevrekidis IG, Panagiotopoulos AZ, et al. Protected peptide nanoparticles: experiments and brownian dynamics simulations of the energetics of assembly. Nano Lett. 2009;9(6):2218–22.
22. Chiou H, Chan HK, Heng D, Prud'homme RK, Raper JA. A novel production method for inhalable cyclosporine A powders by confined liquid impinging jet precipitation. J Aerosol Sci. 2008;39(6):500–9.
23. Gindy ME, Panagiotopoulos AZ, Prud'homme RK. Composite block copolymer stabilized nanoparticles: simultaneous encapsulation of organic actives and inorganic nanostructures. Langmuir. 2008;24(1):83–90.
24. Johnson BK, Prud'homme RK. Flash NanoPrecipitation of organic actives and block copolymers using a confined impinging jets mixer. Aust J Chem. 2003;56(10):1021–4.
25. Kumar V, Hong SY, Maciag AE, Saavedra JE, Adamson DH, Prud'homme RK, et al. Stabilization of the nitric oxide (NO) prodrugs and anticancer leads, PABA/NO and Double JS-K, through incorporation into PEG-protected nanoparticles. Mol Pharm. 2010;7(1):291–8.
26. Kumar V, Wang L, Riebe M, Tung HH, Prud'homme RK. Formulation and stability of itraconazole and odanacatib nanoparticles: governing physical parameters. Mol Pharm. 2009;6(4):1118–24.
27. Liu Y, Tong Z, Prud'homme RK. Stabilized polymeric nanoparticles for controlled and efficient release of bifenthrin. Pest Manag Sci. 2008;64(8):808–12.
28. Shan JN, Budijono SJ, Hu GH, Yao N, Kang YB, Ju YG, et al. Pegylated Composite Nanoparticles Containing Upconverting Phosphors and meso-Tetraphenyl porphine (TPP) for Photodynamic Therapy. Adv Funct Mater. 2011;21(13):2488–95.
29. Shi L, Shan JN, Ju YG, Aikens P, Prud'homme RK. Nanoparticles as delivery vehicles for sunscreen agents. Colloid Surf A. 2012;396:122–9.
30. Han J, Zhu Z, Qian H, Wohl AR, Beaman CJ, Hoye TR, et al. A simple confined impingement jets mixer for flash nanoprecipitation. J Pharm Sci. 2012;101(10):4018–23.
31. Wolak MA, Delcamp J, Landis CA, Lane PA, Anthony J, Kafafi Z. High-performance organic light-emitting diodes based on dioxolane-substituted pentacene derivatives. Adv Func Mater. 2006;16(15):1943–9.
32. Chan HK, Chew NYK. Influence of particle size, air flow, and inhaler device on the dispersion of mannitol powders as aerosols. Pharm Res. 1999;16(7):1098–103.
33. Chapter <601>. United States Pharmacopeia 31 - National Formulary 26: United States Pharmacopeial Convention Inc; 2008.
34. Bronsky EA, Grossman J, Henis MJ, Gallo PP, Yegen U, Della Cioppa G, et al. Inspiratory flow rates and volumes with the Aerolizer dry powder inhaler in asthmatic children and adults. Curr Med Res Opin. 2004;20(2):131–7.
35. Sung JC, Padilla DJ, Garcia-Contreras L, VerBerkmoes JL, Durbin D, Peloquin CA, et al. Formulation and pharmacokinetics of self-

assembled rifampicin nanoparticle systems for pulmonary delivery. Pharm Res. 2009;26(8):1847–55.
36. Sears JT, Huang K, Ray S, Fairbanks HV. Effect of Liquid Properties on Production of Aerosols with Ultrasound. Proceedings, 1977 IEEE Ultrasonics Symposium. 1977:131–3.
37. Geiser M. Update on macrophage clearance of inhaled micro- and nanoparticles. J Aerosol Med Pulm D. 2010;23(4):207–17.
38. Burger A, Henck JO, Hetz S, Rollinger JM, Weissnicht AA, Stottner H. Energy/temperature diagram and compression behavior of the polymorphs of D-mannitol. J Pharm Sci. 2000;89(4):457–68.
39. D'Addio SM, Saad W, Ansell SM, Squiers JJ, Adamson DH, Herrera-Alonso M, et al. Effects of block copolymer properties on nanocarrier protection from in vivo clearance. J Control Release. 2012;162(1):208–17.
40. Nguyen XC, Herberger JD, Burke PA. Protein powders for encapsulation: a comparison of spray-freeze drying and spray drying of darbepoetin alfa. Pharm Res. 2004;21(3):507–14.